A Finite-Time State-Dependent Differential Riccati Equation Control Design for Closed-Loop SMA-Actuated Hip Joint

V. Perez-Sanchez, S. R. Nekoo, B. Arrue, and A. Ollero

***Abstract*—This paper presents the modeling and closed loop control of the shape-memory-alloy (SMA)-actuated hip joint of a flapping-wing flying robot (FWFR). Despite the lightweight legs/claw mechanism, a strong force of grasping is needed. The SMAs show high force delivery; however, it is difficult to control (position and temperature) the actuation due to the necessity of high currents for warming up, and time for cooling down process. This paper presents a state-dependent differential Riccati equation (SDDRE) controller taking into account the SMA dynamic and the actuator limits to control the leg/claw system. The use of nonlinear optimal control, specifically, the SDDRE, has been reported for the first time for bio-inspired leg/claw control of FWFR. The dynamics of the SMA actuators and on-off switching of the MOSFETs to provide current for the system demands switching in the design of the controller as a constraint for inputs which was considered in the design. Simulation and experimental results and analysis of different phases of heating of SMAs were discussed and resulted in satisfactory control performance.**

***Index Terms*—SDRE, SMA, Closed-loop control, Bio-inspired claw, Fkapping-wing robots, UAV, Aerial Robot.**

I. Introduction

THE shape memory alloys (SMA) are made of Nickel Titanium and they are considered as new technology material or smart material. The main applications of SMAs are still under investigation; however, their potential usages, reported in the literature make this material one of the most important candidates for light-weight actuation. One interesting example could indicate the application in the medical domain, implemented in hearing aids transmitting the vibration to the eardrum [1]. In this case, the transition temperature is near the temperature of the human body for recovering the initial shape of the SMA. The main difficulty in working with SMAs is controlling the force. The exerted force by the SMA depends on the deformation and temperature [2], [3]. Usually, the mechanism that controls the heat exchanges is heavy-weight; however, it is interesting to be used in lightweight applications due to its lightweight/high-force ratio of smart materials.

The application of SMAs in this work is the motion control of a very lightweight leg/claw system, installed under a flapping-wing flying robot (FWFR) shown in Fig. 1. The preliminary design and application were reported in [4] though there was no control over the force of the SMAs. Instead, the main objective was to close the claw as tight as possible. The airflow and environment temperature were used to open the claw. A system to release environmental sensors was presented from an unmanned aerial vehicle (UAV) using smart material [5]. On the contrary, in another example SMAs were used to launch a flying system, UAV from trees [6]; it was limited to passive actuation to simplify the workload and the total onboard weight of the system. The position control of a joint using SMA was presented employing a proportional-derivative-integral (PID) design [7]. Two load cells were used to provide closed-loop feedback that is not affordable in lightweight systems and flapping-wing flying platforms.

Fig. 1: The developed SMA actuated hip joint integrated on E-Flap ornithopter [8].

This work implies the design, manufacturing, modeling, and control of a hip joint of an ornithopter. It goes through weight reduction by using SMA actuators. Selecting the smart material for this task, the implementation was constrained by the on-off actuation of the SMAs and adding complexity to the controller and modeling process. The closed-loop controller in this work is the state-dependent differential Riccati equation (SDDRE), reported for the first time for the actuation of SMA installed under flapping-wing robots.

The SDDRE is the differential and finite time version of the state-dependent Riccati equation (SDRE) [9]–[11]. The finite-time option adds more penalty to the end of the control process through the final boundary condition of nonlinear optimal control [12]. The shape memory alloys were used

The authors are with the GRVC Robotics Lab., Departamento de Ingeniería de Sistemas y Automática, Escuela Técnica Superior de Ingeniería, Universidad de Sevilla, Seville, Spain. E-mails: vpsanchez@us.es, saerafee@yahoo.com, barrue@us.es, aollero@us.es

This work was supported by the GRIFFIN Advanced Grant of the European Research Council, Action 788247, and the H2020 AERIAL-CORE project under Grant 871479.

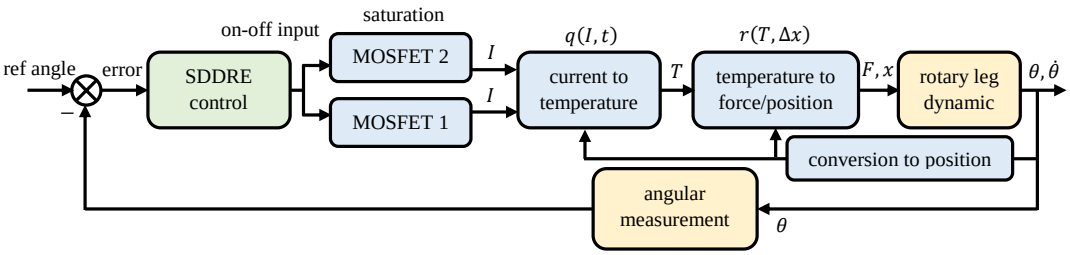

Fig. 2: The block diagram of the control problem of the SMA-actuated system dynamics.

in the SDRE research and literature [13]–[18], briefly reviewed here. Lima et al. presented the SDRE control for positioning of flexible link robots, actuated by SMA material [18]. Simulation results of a three-degree-of-freedom (DoF) planar robot were illustrated. Barzegari et al. investigated the aeroelastic characteristics of the cantilever wing with smart materials employing the SDRE controller [13]. The effect of the SMA actuators on the flutter condition was shown and simulation results were presented to demonstrate the application of smart material in this domain. Naeimifard et al. applied the SDRE controller on position control of a benchmark setup in simulation and experiment [14]. All the valuable mentioned works were solved by an algebraic Riccati equation (SDRE) to find the gain of the controller. In this paper, the differential form SDDRE is simulated and experimented.

Then, the main contributions of this work are 1) Active bi-directional position control of the leg for a flapping-wing flying robot using SMA actuators. 2) Implementing the state-dependent differential Riccati equation for an SMA robotic leg/claw system.

The first contribution adds the closed-loop feedback and pushing/retrieving possibility to the actuator as an important increment advance with respect to Ref. [4], which was preliminary work in this domain without force and position control. The second contribution is related to the application of nonlinear control on smart materials, specifically SMAs. Here the increment contribution is in solving a differential Riccati equation experimentally for closed-loop control in comparison with [13]–[18] where only algebraic SDRE was considered. One of the advantages of the SDDRE is the finite time characteristics that could finish the control task sooner than the SDRE using a weighting matrix of states at the final time.

The paper is structured as follows. In Section II, the system dynamics are modeled. Section III presents the SDDRE control structure. Section IV evaluates the simulation result of the system including the model of Section II and the control structure of Section III. Section V shows the experimental results. Finally, Section VI presents the conclusions of the work.

II. Dynamic Modeling

The dynamics of the ornithopter hip joint system include several parts such as MOSFETs, current to temperature, temperature to force, mechanical section, and feedback measurement components. The MATLAB Simulink software is used to model the system. The control block diagram of the system dynamics is presented in Fig. 2, which shows the arrangement of the different elements. To implement the SDRE nonlinear optimal controller, the first step is to develop the dynamic equations to model the SMA actuators.

The SMAs are special Nickel and Titanium alloys that change their phase between martensite and austenite depending on the temperature. There are two main temperatures to analyze the behavior of the SMA. The first is the pure martensite temperature and the second is the pure austenite temperature. Then the transition is linear from one phase to another. The SMA behavior was studied in terms of the stress and the phase [3]. A model was proposed to obtain the generated force by the alloy as a function of the elongation and the phase of the alloy was proposed [2].

Concerning the developed SMA system, the actuation starts in a de-twined martensite state evolving to austenite with the raise of the temperature. The applied initial force by the SMA could be modeled as the needed force to perform a plastic deformation in the martensitic state. That simplifies the actuation model reducing the discontinuities and evaluating the evolution of the alloy during the change of phases.

The application requires a well-developed model of the alloy that shows the properties during the operations with the fixed condition. It is proposed to obtain the generated force by the alloy through:

$$r(T,x) = F_{\mathrm{PD}} + K\Delta T\Delta x, \tag{1}$$

where F_{PD} is the identified stress to perform a plastic deformation in the martensite phase of the alloy, K is the phase-change constant, ΔT is the variation of temperature and Δx is the elongation of the spring. The proposed method is based on the antagonist muscles configuration, presented in Fig. 3, right side. In this configuration, the generated force by one spring is directly opposed to the other. That makes it possible to simplify the model assuming that the spring is at least in the de-twined martensite phase, which is identified by F_{PD}, adding the generated force to that by the change of phase and the elongation.

The value of F_{PD} could be found by extending the spring on the martensite phase against a load cell and discharging the transition on the force. The gradient of curve K was iden-

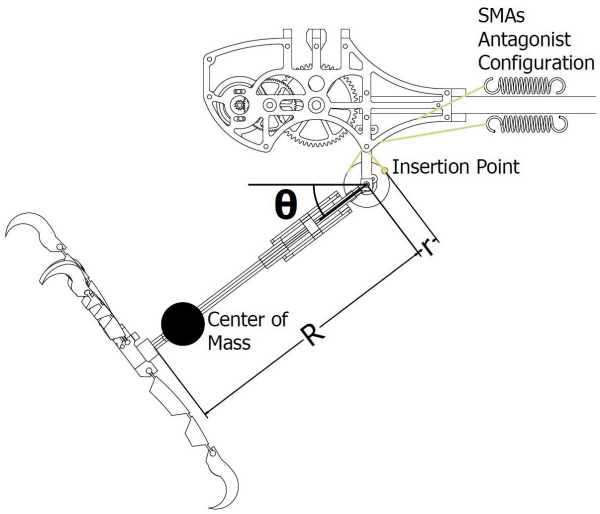

Fig. 3: The physical representation of the model.

tified by varying the temperature with different elongations and analyzing the relationship. The model works between the plastic deformation in the martensite/austenitic phases. By evaluating the evolution of F_{PD}, the fatigue of the spring could be obtained.

To find the dynamics of the heat exchange, the stored energy in the spring is evaluated:

$$E_{\mathrm{spring}}(I,t,T) = \int_{t(T_0)}^{t(T)} [P_{\mathrm{c}}(I) - P_{\mathrm{L}}(T)]\mathrm{d}t, \tag{2}$$

where $E_{\mathrm{spring}}(I,t,T)$ is the stored energy in the spring, $P_{\mathrm{c}}(I)$ is the total electrical consumed power by the whole system in terms of the current, and $P_{\mathrm{L}}(T)$ is the instant power loss depending on the temperature. The integration limits are between the time in which the temperature is T_o and the unknown time in which the temperature reaches T.

$P_{\mathrm{c}}(I)$ have been estimated from the electrical analysis of the spring. Several tests were conducted to implement these equations. The first step was to analyze the power consumption of the spring by applying different electrical currents to obtain the equivalent electrical resistor. Fig. 4 shows the electrical behavior of the spring, temperature, and current. It shows the temperature in terms of the time on the left and the power consumption on the right.

Analyzing the power consumption in terms of the temperature, it could be observed that the behavior is constant. Consequently, the internal equivalent resistor of the spring is also constant. The value was obtained from the relationship between power consumption and the applied current. Identifying electrically the system. The electrical power consumption could be expressed as follows:

$$P_{\mathrm{c}}(I) = I^2 R_{\mathrm{spring}}, \tag{3}$$

where I is the electrical current applied to the system, R_{spring} is the identified equivalent resistor of the spring.

The thermal and electrical analyses were combined to calculate the delivered energy to the air. Fig. 4 shows a limit

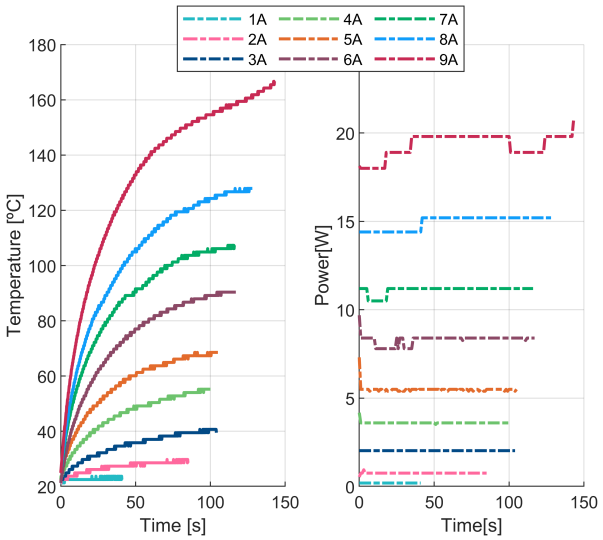

Fig. 4: Electrical behavior of the SMA in time and terms of energy consumption. Left side temperature time dependency. Right side power consumption

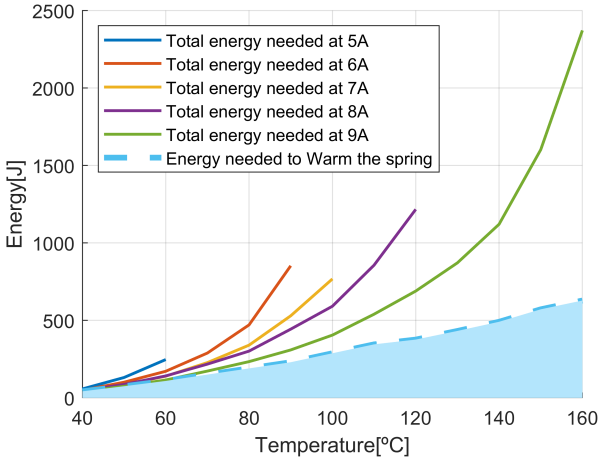

Fig. 5: The SMA Spring energy consumption. The graphic shows shaded in blue limited by a dashed line the useful energy. The continuous lines represent the consumed energy in different colors in terms of the applied current.

in the temperature in terms of the current. On the limit, all the applied power to the spring is transferred to the environment. That makes it possible to identify the energy losses in terms of the spring temperature and environment temperature. Fig. 5 evaluates graphically the results.

Analyzing the results, heat transfer is linear in terms of temperature. Evaluating it in a theoretical way, it could be modeled as a resistor delivering energy to the environment. So the energy loss is modeled through the convection mechanism of heat transfer as follows:

$$P_{\mathrm{L}} = hA(T - T_0), \tag{4}$$

where h is the heat transfer coefficient and A is the contact area with the air.

It is difficult to determine the heat transfer coefficient and the contact area of the system. Regarding the contact area, the system has a lot of components supporting a high current.

It is impractical to consider all the components theoretically, therefore, these parameters and the heat transfer coefficient were identified by using the analytical data. Regarding the results of the electrical analysis, the wasted energy on the spring is defined. The graphic shows the total consumed energy in terms of the current and shaded the useful energy, Fig. 5. By evaluating these equations the stored energy in the spring depending on the time, current, and environment temperature, is obtained, and $q(I,t)$ is defined.

The next step is to obtain the equations that define the movement of the joint and the relationship with the generated forces by the SMA springs in the antagonist configuration. Fig. 3 shows a simplification of the system in which the main parameter of the system has been highlighted. The actuation system is composed of two SMA springs in an antagonist configuration. The generated forces by the SMA system are transmitted to the hip joint by using tendons and a pulley to guarantee the moment generation. The pulley is directly connected to the leg of the system. The mass of the end-effector (claw) and the leg have been substituted by a mass in the center of mass of the leg/end-effector system. To evaluate this system, Euler-Lagrange has been applied using the general coordinate θ. The displacement of the spring is obtained regarding that the tensor is always in contact with the internal surface of the pulley. The friction of the joint has been considered as well. Equation 5 shows the dynamic behavior of the system:

$$(I_{zz}+M_{\text{eq}}R_{\text{CoG}}^2)\ddot{\theta}(t)-M_{\text{eq}}R_{\text{CoG}}g\sin\theta(t)=\sum F_{\text{SMA}}(t)r-c\dot{\theta}(t), \quad (5)$$

where $M_{\text{eq}}(\text{kg})$ is the equivalent mass of the system in the center of gravity (CoG), $I_{zz}(\text{kg.m}^2)$ is the moment of inertia of the leg, $R(\text{m})$ is the distance from the rotational point to the CoG, $g=9.81(\text{m/s}^2)$ is the gravity constant, $\theta(t)(\text{rad})$ is the generalized coordinate of the system, $\sum F(\text{N})$ is the resultant of the forces of the SMA spring in antagonist configuration, $r(\text{m})$ is the internal radius of the pulley and $c(\text{kg.m/s})$ is the dynamic friction coefficient. The input parameters to the system are the input current of the active spring and the antagonist spring. The output of the evaluated system is the position of the leg measured by a potentiometer, $\theta(t)$. All the subsystems have been modeled theoretically to proceed with the design and simulation of the controller before starting the experimental validation. Considering the state-vector of the system as $\mathbf{x}(t)=[\theta(t),\dot{\theta}(t)]^\top$, the state-space representation of the mechanical part is found:

$$\dot{\mathbf{x}}(t)=\begin{bmatrix}0 & 1\\ \frac{M_{\text{eq}}R_{\text{CoG}}g\sin x_1(t)}{(I_{zz}+M_{\text{eq}}R_{\text{CoG}}^2)x_1(t)} & \frac{-c}{I_{zz}+M_{\text{eq}}R_{\text{CoG}}^2}\end{bmatrix}\mathbf{x}(t)+\begin{bmatrix}0\\ \frac{1}{I_{zz}+M_{\text{eq}}R_{\text{CoG}}^2}\end{bmatrix}\sum F_{\text{SMA}}(t)r. \quad (6)$$

III. The SDDRE Control Structure

Consider a nonlinear time-invariant affine-in-control system in the form of:

$$\dot{\mathbf{x}}(t)=\mathbf{f}(\mathbf{x}(t))+\mathbf{g}(\mathbf{x}(t),\mathbf{u}(t)), \quad (7)$$

where $\mathbf{x}(t)\in\mathbb{R}^n$ is the state vector of the system, $\mathbf{u}(t)\in\mathbb{R}^m$ is the input vector. $\mathbf{f}(\mathbf{x}(t)):\mathbb{R}^n\to\mathbb{R}^n$ and $\mathbf{g}(\mathbf{x}(t),\mathbf{u}(t)):\mathbb{R}^n\times\mathbb{R}^m\to\mathbb{R}^n$ are vector-valued smooth piecewise-continuous functions that satisfy the Lipschitz condition.

System (7) is transformed to state-dependent coefficient (SDC) parameterization:

$$\dot{\mathbf{x}}(t)=\mathbf{A}(\mathbf{x}(t))\mathbf{x}(t)+\mathbf{B}(\mathbf{x}(t))\mathbf{u}(t), \quad (8)$$

where $\mathbf{A}(\mathbf{x}(t)):\mathbb{R}^n\to\mathbb{R}^{n\times n}$ and $\mathbf{B}(\mathbf{x}(t)):\mathbb{R}^n\to\mathbb{R}^{n\times m}$ are held.

Condition 1. The pair of $\{\mathbf{A}(\mathbf{x}(t)),\mathbf{B}(\mathbf{x}(t))\}$ is a controllable parameterization of system (7) for all $\mathbf{x}(t)\in\mathbb{R}^n$ in $t\in\mathbb{R}^+$ [19].

Considering the state-space (6), the SDC matrices are defined as:

$$\mathbf{A}(\mathbf{x}(t))=\begin{bmatrix}0 & 1\\ \frac{M_{\text{eq}}R_{\text{CoG}}g\left(1-\frac{x_1^2(t)}{6}+\frac{x_1^4(t)}{120}-\cdots\right)}{I_{zz}+M_{\text{eq}}R_{\text{CoG}}^2} & \frac{-c}{I_{zz}+M_{\text{eq}}R_{\text{CoG}}^2}\end{bmatrix},\quad \mathbf{B}=\begin{bmatrix}0\\ \frac{1}{I_{zz}+M_{\text{eq}}R_{\text{CoG}}^2}\end{bmatrix}, \quad (9)$$

in which $\sin x_1(t)$ is replaced with its Taylor series expansion, $x_1(t)-\frac{x_1^3(t)}{6}+\frac{x_1^5(t)}{120}-\cdots$, to omit the denominator $x_1(t)$ in the SDC matrices and avoid singularity when $x_1(t)=0$.

The cost function integral of the SDRE (sub-optimal controller) is defined [20]:

$$J=\frac{1}{2}\mathbf{x}^\top(t_{\text{f}})\mathbf{F}\mathbf{x}(t_{\text{f}})+\frac{1}{2}\int_0^{t_{\text{f}}}\{\mathbf{x}^\top(t)\mathbf{Q}(\mathbf{x}(t))\mathbf{x}(t)+\mathbf{u}^\top(t)\mathbf{R}(\mathbf{x}(t))\mathbf{u}(t)\}\,\text{d}t, \quad (10)$$

where $\mathbf{Q}(\mathbf{x}(t)):\mathbb{R}^n\to\mathbb{R}^{n\times n}$ is the weighting matrix of states and $\mathbf{R}(\mathbf{x}(t)):\mathbb{R}^n\to\mathbb{R}^{m\times m}$ is the one for the inputs, symmetric positive semi-definite and definite, respectively. $\mathbf{F}\in\mathbb{R}^{n\times n}$ is the weighting matrix of states at final time $t_{\text{f}}(\text{s})$.

Condition 2. The pair of $\{\mathbf{A}(\mathbf{x}(t)),\mathbf{Q}^{1/2}(\mathbf{x}(t))\}$ is an observable parameterization of system (7) for all $\mathbf{x}(t)\in\mathbb{R}^n$ in $t\in\mathbb{R}^+$ in which $\mathbf{Q}^{1/2}(\mathbf{x}(t))$ is the Cholesky decomposition of $\mathbf{Q}(\mathbf{x}(t))$ [9].

The control law of the SDRE is presented as:

$$\mathbf{u}(t)=-\mathbf{R}^{-1}(\mathbf{x}(t))\mathbf{B}^\top(\mathbf{x}(t))\mathbf{K}(\mathbf{x}(t))\mathbf{x}(t), \quad (11)$$

where $\mathbf{K}(\mathbf{x}(t)):\mathbb{R}^n\to\mathbb{R}^{n\times n}$ is the symmetric positive-definite solution to the state-dependent differential Riccati equation (SDDRE) [21]:

$$\mathbf{A}^\top(\mathbf{x}(t))\mathbf{K}(\mathbf{x}(t))+\mathbf{K}(\mathbf{x}(t))\mathbf{A}(\mathbf{x}(t))-\mathbf{K}(\mathbf{x}(t))\mathbf{B}(\mathbf{x}(t))\mathbf{R}^{-1}(\mathbf{x}(t))\mathbf{B}^\top(\mathbf{x}(t))\mathbf{K}(\mathbf{x}(t))+\mathbf{Q}(\mathbf{x}(t))=-\dot{\mathbf{K}}(\mathbf{x}(t)), \quad (12)$$

where the final boundary condition of the differential equation is $\mathbf{K}(\mathbf{x}(t_f)) = \mathbf{F}$. There are several solution methods for SDDRE (12), studied in Ref. [21]; here to solve the SDDRE, Lyapunov-based method is used via negative root to Riccati equation [9]. The first step is to solve the SDRE:

$$\mathbf{A}^\top(\mathbf{x}(t))\mathbf{K}_{ss}^-(\mathbf{x}(t)) + \mathbf{K}_{ss}^-(\mathbf{x}(t))\mathbf{A}(\mathbf{x}(t)) - \mathbf{K}_{ss}^-(\mathbf{x}(t))\mathbf{B}(\mathbf{x}(t))\mathbf{R}^{-1}(\mathbf{x}(t))\mathbf{B}^\top(\mathbf{x}(t))\mathbf{K}_{ss}^-(\mathbf{x}(t)) + \mathbf{Q}(\mathbf{x}(t)) = \mathbf{0}, \quad (13)$$

and find its negative root where $\mathbf{K}_{ss}^-(\mathbf{x}(t)) : \mathbb{R}^n \to \mathbb{R}^{n\times n}$ is the negative-definite steady-state solution to (13). The next step is to define a closed-loop matrix:

$$\mathbf{A}_{cl}(\mathbf{x}(t)) = \mathbf{A}(\mathbf{x}(t)) - \mathbf{B}(\mathbf{x}(t))\mathbf{R}^{-1}(\mathbf{x}(t))\mathbf{B}^\top(\mathbf{x}(t))\mathbf{K}_{ss}^-(\mathbf{x}(t)),$$

and solving state-dependent differential Lyapunov equation:

$$\dot{\mathbf{P}}(\mathbf{x}(t)) = \mathbf{A}_{cl}(\mathbf{x}(t))\mathbf{P}(\mathbf{x}(t)) + \mathbf{P}(\mathbf{x}(t))\mathbf{A}_{cl}^\top(\mathbf{x}(t)) - \mathbf{B}(\mathbf{x}(t))\mathbf{R}^{-1}(\mathbf{x}(t))\mathbf{B}^\top(\mathbf{x}(t)), \quad (14)$$

with final boundary condition $\mathbf{P}(\mathbf{x}(t_f)) = \{\mathbf{F} - \mathbf{K}_{ss}^-(\mathbf{x}(t))\}^{-1}$. The solution to (14) is found by solving algebraic Lyapunov equation:

$$\mathbf{A}_{cl}(\mathbf{x}(t))\mathbf{E}(\mathbf{x}(t)) + \mathbf{E}(\mathbf{x}(t))\mathbf{A}_{cl}^\top(\mathbf{x}(t)) = \mathbf{B}(\mathbf{x}(t))\mathbf{R}^{-1}(\mathbf{x}(t))\mathbf{B}^\top(\mathbf{x}(t)),$$

and substituting $\mathbf{E}(\mathbf{x}(t))$ into the closed-form solution:

$$\mathbf{P}(\mathbf{x}(t)) = \mathbf{E}(\mathbf{x}(t)) + \exp\{\mathbf{A}_{cl}(\mathbf{x}(t))(t-t_f)\}[\mathbf{P}(\mathbf{x}(t_f)) - \mathbf{E}(\mathbf{x}(t))]\exp\{\mathbf{A}_{cl}^\top(\mathbf{x}(t))(t-t_f)\},$$

that generates the final answer, a symmetric positive-definite solution to the SDDRE (12) $\mathbf{K}(\mathbf{x}(t)) = \mathbf{K}_{ss}^-(\mathbf{x}(t)) + \mathbf{P}^{-1}(\mathbf{x}(t))$. So, by defining the SDC matrices, (8), and replacing them into the differential Riccati equation (12), the control gain is found and substituted into the control law (11). Then the input law will regulate the system (7) to the equilibrium point. It should be noted that the SDDRE control design is subjected to on-off actuation, peculiar to the real actuation of SMA and MOSFETs in this work. The control law is constrained by:

$$\mathbf{u}(t) = \begin{cases} \mathbf{u}_{max}\,\text{sign}(\mathbf{u}(t)) & |\mathbf{u}(t)| > \mathbf{u}_{threshold}, \\ \mathbf{0} & |\mathbf{u}(t)| < \mathbf{u}_{threshold}, \end{cases} \quad (15)$$

in which $\text{sign}(\cdot)$ is the signum function, $\mathbf{u}_{max}$ is the maximum limit of the input signal, and $\mathbf{u}_{threshold}$ is the threshold value that defines the switching between the input bounds.

IV. Simulation

The Simulink model has been built based on the presented equations and dynamics in Section II and Fig. 2. The input of the model is the supplied voltage to the spring. The electrical model sets the applied current to each spring. The thermal model, Eq. (2), receives the provided current to the spring and emulates the exchanges of energy with the air. The spring dynamic model Eq. (1) generates the applied force by the spring in terms of elongation and temperature. Finally, the dynamics of both springs are combined for actuation in the joint in Eq. (5). The parameters of the simulation are presented in Table I.

TABLE I: The parameters of the simulation and the model.

Parameter	Value	Unit
Environment temperature	298	K
Voltage supply	3	V
Current supply	13.31	A
R Eq.2	0.2253	Ω
F_{PD} Eq.1	0.4286	N
K Eq.1	2.1096	N/m
Gravity constant	9.81	m/s^2

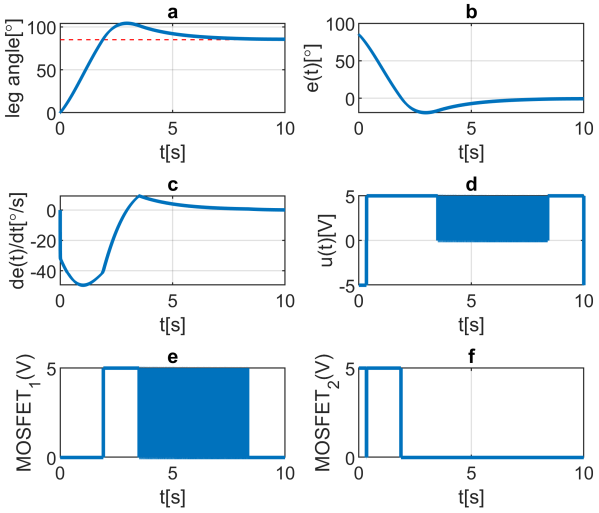

Fig. 6: The simulation results of the model in Simulink and regulation from initial to final condition.

The initial condition of the leg is set at zero degree, $\theta(0) = 0^\circ$ and the final condition is chosen $\theta(t_f) = 85^\circ$. The final time of simulation is set $t_f = 10(\text{s})$. The maximum voltage of the input is $u_{max} = V_{max} = 5(\text{V})$ and the threshold voltage is $u_{threshold} = V_{threshold} = 0.01(\text{V})$. The center-of-mass of the leg is $R_{CoG} = 0.0504(\text{m})$, mass of the leg is $M_{eq} = 0.053(\text{kg})$, the moment of inertia is $I_{zz} = 190.274 \times 10^{-6}(\text{kg.m}^2)$, and friction constant is $c = 0.01(\text{kg.m/s})$. Considering the weighting matrices as $R = 1$, $\mathbf{Q} = \text{diag}(10, 30)$, and $\mathbf{F} = 50 \times \mathbf{Q}$, results in the convergence of the error to zero, which was the objective of the control design. The generalized coordinate, error, and error velocity are illustrated in Fig. 6-(a-c). The on-off input of the SDRE is illustrated in Fig. 6-(d), and the input signals to MOSFETs are shown in Fig. 6-(e-f), switching between $0 - 5(\text{V})$. The convergence rate of error is showing a favorable result.

V. Experiments

The experimental setup of the leg/claw system, installed under a flapping-wing robot is illustrated in Fig. 7a. It is divided into two parts; the setup for the representation is shown on the left side and the setup on board is shown

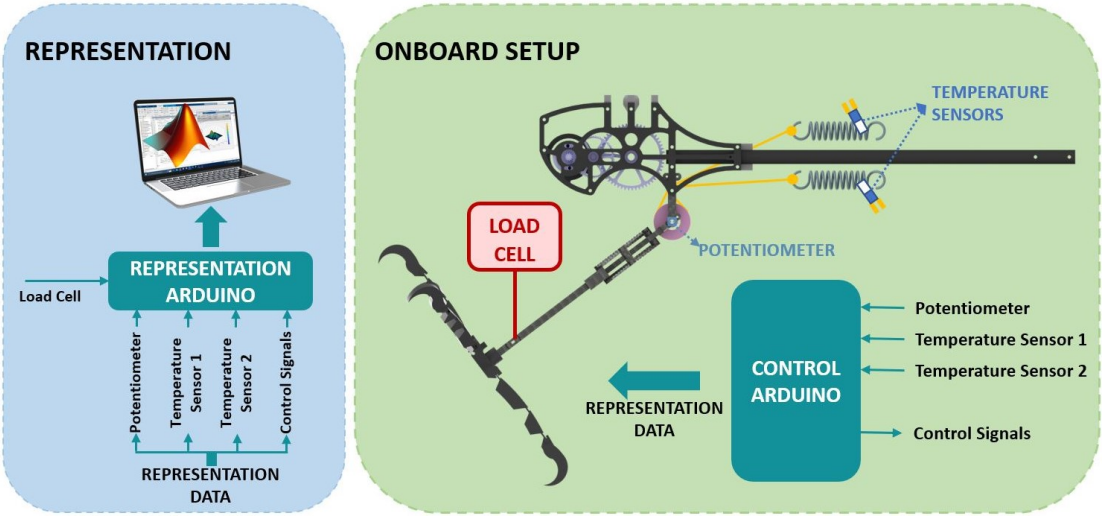

(a) The diagram of the experimental setup with graphical representation.

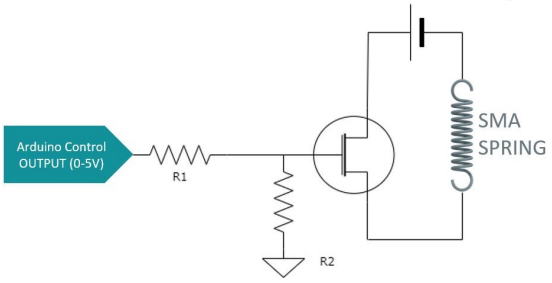

(b) Control outputs to SMA springs.

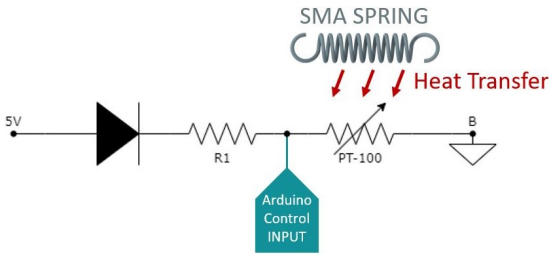

(c) Control input.

Fig. 7: The experimental setup and control signals.

on the right side. The objective of this configuration is to avoid possible non-modeled delays of the representation in the behavior of the system.

The dynamic model is based on the experimental results to generate comparable data. Also, the electronics to control the system have been taken into account in Section IV. The feedback to the control system is the position and velocity of the joint and the temperature of the spring. The input control computed by the SDDRE is the applied current to the SMA spring. The actuation comprises two springs for forward and backward motions in an antagonistic configuration. The selected SMA spring was custom-made from a wire of 1.5mm in diameter. Firstly, the wire was deformed in a spring shape in a local factory. Then a thermal treatment was performed in the GRVC laboratory maintaining the spring shape for 1 hour at 450ºC. Ultimately, the spring has a coil diameter of 15mm and 4.5g of weight. They can exert forces up to 100N with an elongation that is 3.5 times bigger than the initial state and 120ºC of temperature. Another important part of the setup is the spring installation and the initial elongations. The initial elongation of the spring set the position of the joint at 180º or 0º. Spring 1 is compressed at 0º; however, it still has to exert force to reach this position to balance with spring 2. Due to that, the initial longitude of spring 1 is 20mm, 30% bigger than the initial longitude of the spring. At 180º spring 1 has an elongation of 58mm. The movement of spring 2 is opposed to spring 1 in terms of the angle. The configuration was also used in sections IV and II.

Kevlar tendons were used to transmit the force of the SMAs configuration to the joint. This material can support the temperature of the spring while having great stress resistance. The force is transmitted to a pulley that connects the SMA system and the hip joint. The weight of the leg and friction have been considered in the model in Section IV, making it possible to test the system's viability.

The SDDRE controller has been implemented into an *Arduino board* to manage the actuation. The control inputs have fed the SMA springs through MOSFETs to manage the high current. The electrical diagram to control the actuation of the spring is shown in Fig. 7b. There are two control outputs and circuits to manage separately the actuation of each spring.

Arduino manages to have a digital output of either 0V or 5V. This output is inserted in the gate of the MOSFET that switches on and off the actuation. This configuration aims to deliver as much current as possible to the SMA, reducing the heating time. However, the control is more complex because of the increased inertia of the system. To control the temperature of the alloy, a PT-100 sensor was used. The diagram in Fig. 7c shows the connection of the sensor.

A tension divider was used to measure the variation of the PT-100 voltage with the temperature. *Arduino* receives

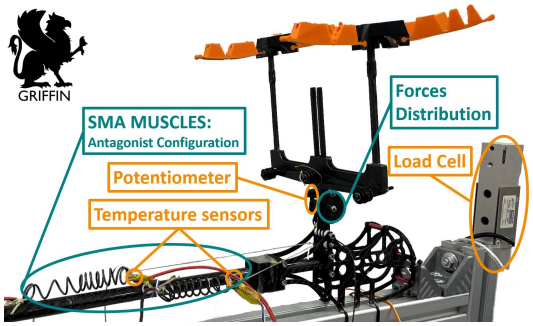

Fig. 8: Real experimental setup. This figure shows all the systems integrated into the ornithopter ready for the experiment.

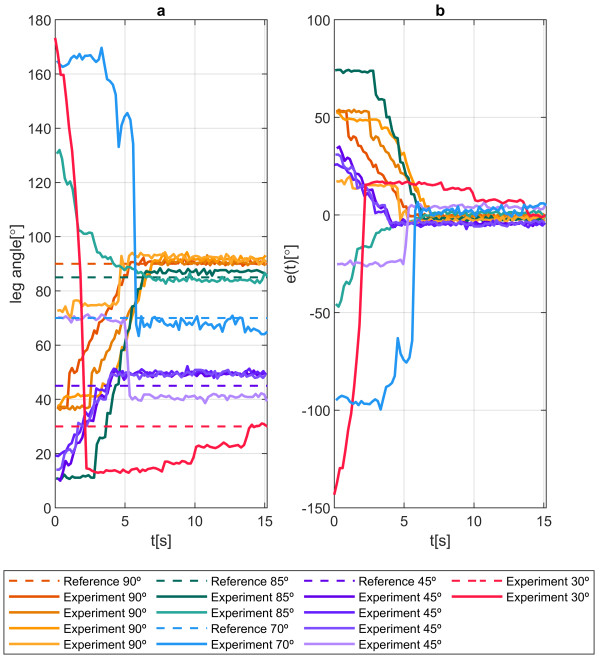

Fig. 9: Experiment summary. The experiments with the same reference have been represented in the same range of colors. (a) shows in the dashed line the different references and continuous the actual position. (b) shows the error between the reference and the actual position.

the voltage consumed by the sensor and calculates the electrical resistor of the sensor. The temperature is obtained by evaluating this data in the temperature/electrical curve of the resistor provided by the manufacturer. As shown in Section II, knowing the state of the temperature, it is possible to reduce the fatigue of the alloy. That makes it possible to improve the number of cycles the SMA can afford without losing properties.

The last input to the controller is the position, and a potentiometer was used to measure the leg's position. The resistor of the potentiometer varies depending on the position given a voltage to the *Arduino* input. This voltage is computed to have the position of the leg. To avoid the cost of the representation in terms of time, an external *Arduino* was used to receive the signal given by the controller and sensors. This data was used for the representation of the experiments. Fig. 8 shows a picture highlighting the system's main component.

Figure 8 shows the real integration of the system presented

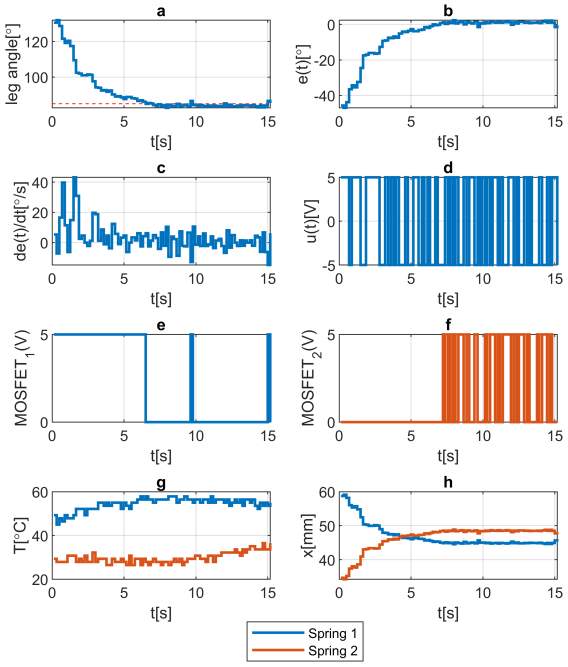

Fig. 10: Experimental validation reference angle 85°. (a) shows the representation of the position with the time, (b) and (c) show the error and the derivative error, (d) shows the input signal of the SDRE controller, (e) and (f) show the control signal to the spring 1 and spring 2 respectively, (g) shows the temperature of the springs, and (h) shows the elongation of the spring.

in the schematic view in Fig. 7a. This figure shows the antagonist SMA configuration of the muscles, having the distribution of the forces on the pulley. The temperature sensors are also shown. The contact area of the sensors is 2×5mm. They are surrounded by silver-based glue to guarantee thermal conductivity and their position on the spring. The figure also shows the position of the potentiometer in the axle of the hip joint, guaranteeing a good measure. The load cell in the figure was used for the modeling process of the system. Fig. 9 summarizes the experiments with different inputs and starting points.

Five references were achieved to test the behavior of the controller and the system. For each reference, different starting points were tested. The change in the initial point makes it reach the equilibrium in the position with different temperature values. It is important to test this because the relationship with the temperature is not trivial. That makes it possible to test whether the system works correctly in distinct configurations. As shown in Fig. 9, the control system is working with good behavior, going to the reference and reducing the error. Also, the response time is similar to the one exposed in Section IV. Fig. 10 focuses on one experiment to show all the values given by the data of the experiments.

Fig. 10-(a) shows the system going to the reference. The time to reach the reference is the same as the one observed during the system simulation. Fig. 10-(b) and -(c) show the system reducing the error. Fig. 10-(e), -(f), -(g), and -(h) are directly related to the behavior of the springs. The disparity between Figure 6 and Figure 10 is due to the initial conditions

of the experiments. In the model results, the spring's initial condition is at the environment temperature, and the initial position is 0°. However, the controller demonstrated that it can respond to varying initial conditions.

When comparing the SDDRE controller with other classical control methods (such as PD/PID) the overshoot is smaller. The comparison of the SDDRE with respect to SDRE also confirmed the effectiveness of the differential form in finite time control. The SDDRE can properly model the actuation to reduce the equilibrium temperature and increase the number of cycles the spring can support. It is also good for the electronics reducing the switching in the equilibrium. In terms of efficiency, the SMA also reduces the consumption of energy. This is important in lightweight platforms due to the weight of the batteries, which sometimes is a great part of the total weight of the platform. On the FWFR platform, weight is one of the most important properties. It is different to have maneuverability during the flight or not. For that reason, the miniaturization of the systems in this paper plays an important role.

VI. Conclusions

This work presented the application of smart material in building a robotic leg/claw for a very lightweight platform, a flapping-wing flying robot. This robot has a very limited load-carrying capacity, and any weight reduction adds value to the design and the method. The shape memory alloys are a good choice for actuating the bio-inspired setups and produce significant force comparing the weight of the actuator. The difficulty in SMA control is controlling the temperature, force, and position to carry out the task. Here the model of the system was presented, and the state-dependent differential Riccati equation was used to control the robotic bio-inspired leg/claw system. The results, temperature analysis, and experimental outputs validated the proposed controller's performance and showed the SDDRE's compatibility for onboard computations.

VII. Acknowledgment

We thank our colleagues Carlos Pajuelo Rojo and Jorge Rodriguez Rubio for their contributions. This work was supported by the GRIFFIN Advanced Grant of the European Research Council, Action 788247, the AERIAL-CORE H2020 project under Grant 871479, and the project "Robótica inteligente para Servicios Espaciales en Órbita (AROSA)," reference number CPP-2021-008629, funded by the Spanish Ministry of Science and Innovation.

References

[1] D. Beutner and K.-B. Hüttenbrink, "Passive and active middle ear implants," *GMS current topics in otorhinolaryngology, head and neck surgery*, vol. 8, 2009.

[2] S. Kim, E. Hawkes, K. Choy, M. Joldaz, J. Foleyz, and R. Wood, "Micro artificial muscle fiber using niti spring for soft robotics," in *2009 IEEE/RSJ International Conference on Intelligent Robots and Systems*, pp. 2228–2234, 2009.

[3] C. Liang and C. Rogers, "Design of shape memory alloy springs with applications in vibration control," *Journal of Vibration and Acoustics*, 1993.

[4] A. E. Gomez-Tamm, V. Perez-Sanchez, B. C. Arrue, and A. Ollero, "Sma actuated low-weight bio-inspired claws for grasping and perching using flapping wing aerial systems," in *2020 IEEE/RSJ International Conference on Intelligent Robots and Systems (IROS)*, pp. 8807–8814, 2020.

[5] L. Pellone, S. Ameduri, N. Favaloro, and A. Concilio, "Sma-based system for environmental sensors released from an unmanned aerial vehicle," *Aerospace*, vol. 4, no. 1, 2017.

[6] A. Farinha, R. Zufferey, P. Zheng, S. F. Armanini, and M. Kovac, "Unmanned aerial sensor placement for cluttered environments," *IEEE Robotics and Automation Letters*, vol. 5, no. 4, pp. 6623–6630, 2020.

[7] M. Moallem and V. A. Tabrizi, "Tracking control of an antagonistic shape memory alloy actuator pair," *IEEE Transactions on Control Systems Technology*, vol. 17, no. 1, pp. 184–190, 2009.

[8] R. Zufferey, J. Tormo-Barbero, M. M. Guzmán, F. J. Maldonado, E. Sanchez-Laulhe, P. Grau, M. Pérez, J. Á. Acosta, and A. Ollero, "Design of the high-payload flapping wing robot e-flap," *IEEE Robotics and Automation Letters*, vol. 6, no. 2, pp. 3097–3104, 2021.

[9] S. R. Nekoo, "Tutorial and review on the state-dependent riccati equation," *Journal of Applied Nonlinear Dynamics*, vol. 8, no. 2, pp. 109–166, 2019.

[10] M. H. Korayem and N. Y. Lademakhi, "Integrated nonlinear suboptimal control-and-estimator based on the state-dependent differential riccati equation approach," *Optimal Control Applications and Methods*, 2022.

[11] A. A. Kabanov, "Finite-time state-dependent coefficient method for optimal control of nonlinear systems," in *2022 International Conference on Industrial Engineering, Applications and Manufacturing (ICIEAM)*, pp. 717–721, IEEE, 2022.

[12] B. Geranmehr, K. Vafaee, and S. Rafee Nekoo, "Finite-horizon servo sdre for super-maneuverable aircraft and magnetically-suspended cmgs," *Proceedings of the Institution of Mechanical Engineers, Part G: Journal of Aerospace Engineering*, vol. 230, no. 6, pp. 1075–1093, 2016.

[13] M. M. Barzegari, M. Dardel, and A. Fathi, "Control of aeroelastic characteristics of cantilever wing with smart materials using state-dependent riccati equation method," *Journal of Intelligent Material Systems and Structures*, vol. 26, no. 8, pp. 988–1005, 2015.

[14] A. Naeimifard and A. Ghanbarzadeh, "Optimal position control of shape memory alloys actuator with nonlinear behavior by using states dependent riccati equation (sdre)," *International Journal of Nonlinear Analysis and Applications*, 2022.

[15] F. C. Janzen, "Positioning and vibration control of a flexible structure in slewing motion by applying shape memory alloys," *Thesis*, 2016.

[16] F. C. Janzen, Â. M. Tusset, V. Piccirillo, J. M. Balthazar, B. R. de Pontes Jr, M. Silveira, and R. M. Brasil, "Control of slewing motions of flexible structures using shape memory alloy," in *ASME International Mechanical Engineering Congress and Exposition*, vol. 46483, p. V04BT04A028, American Society of Mechanical Engineers, 2014.

[17] A. M. Tusset, F. C. Janzen, V. Piccirillo, and J. M. Balthazar, "Slewing control of flexible space structures: on state dependent ricatti equations approach," in *Proceedings of the XXXIV Iberian Latin-American Congress on Computational Methods in Engineering*, 2013.

[18] J. J. d. Lima, A. M. Tusset, F. C. Janzen, V. Piccirillo, C. B. Nascimento, J. M. Balthazar, and R. M. L. R. d. F. Brasil, "Sdre applied to position and vibration control of a robot manipulator with a flexible link," *Journal of Theoretical and Applied Mechanics*, vol. 54, no. 4, pp. 1067–1078, 2016.

[19] S. R. Nekoo, "Digital implementation of a continuous-time nonlinear optimal controller: An experimental study with real-time computations," *ISA transactions*, vol. 101, pp. 346–357, 2020.

[20] S. R. Nekoo, J. Á. Acosta, and A. Ollero, "Gravity compensation and optimal control of actuated multibody system dynamics," *IET Control Theory & Applications*, vol. 16, no. 1, pp. 79–93, 2022.

[21] M. H. Korayem and S. Nekoo, "Finite-time state-dependent riccati equation for time-varying nonaffine systems: Rigid and flexible joint manipulator control," *ISA transactions*, vol. 54, pp. 125–144, 2015.